A Friction Model-Based Frequency Response Analysis for Frictional Servo Systems

Yoshihiro Maeda, *Member, IEEE,* Kazuya Harata, *Non-member,* and Makoto Iwasaki, *Fellow, IEEE*

***Abstract*—This paper presents a friction model-based frequency response analysis (FRA) method which gives a precise linear mechanical dynamics model to design effective controllers and analyze accurate control characteristics for frictional servo systems. As well known, frequency-domain identification approaches using a sine sweep are widely used to obtain linear dynamics. However, nonlinear friction in the mechanism varies the apparent frequency-domain characteristic of the linear dynamics due to the nonlinearity. The proposed FRA estimates effective excitation thrust for actual linear dynamics in the sine sweep movement, by means of a friction model as well as a phase delay model. Theoretical analyses show that the proposed FRA can identify the correct linear dynamics, preventing influence of nonlinear friction as well as phase delay properties included in a plant system. The effectiveness of the proposed FRA is verified through theoretical analyses and experiments both in frequency and time domains, in comparison to two conventional FRA methods.**

***Index Terms*—Frequency response analysis, frequency-domain identification, rolling friction, linear plant dynamics, phase delay, observer.**

I. Introduction

In order to achieve high productivity and high quality of products, the fast and precise positioning control is one of key technologies in industrial mechatronic systems, such as semiconductor fabrication machines, data storage devices, electronics manufacturing machines, machine tools, etc [1]−[3]. Recently, the servo mechanisms are getting low rigidity because of weight saving and cost reduction, which lead to unfavorable vibratory responses due to lower mechanical resonant frequencies [4]−[6]. In order to achieve the high-performance positioning with vibration suppression capabilities, the two-degree-of-freedom (2DoF) control framework is effective and widely-used [7]−[9], while system identification for "*linear*" mechanical dynamics is becoming more important for an effective controller design [10], [11].

In general, actual servo systems such as linear motor-driven and/or ball screw-driven tables have "*nonlinear*" friction at ball screw nuts, bearings, and linear guideways. For instance, the rolling friction generated at contact points between rolling elements and guides shows nonlinear phenomena, which behave quite differently between macro- and micro-displacement regions [12]. Since the complicated nonlinear friction causes undesired position responses, various research works have been done, focusing on friction compensation and analyses [10], [13]−[17]. On the other hand, it is well-known that the nonlinear properties affect the system identification based on frequency response analysis (FRA) methods [12], [18]−[20]. The frequency-domain identification is commonly used to obtain useful information of the linear dynamics (e.g., mass, moment of inertia, and resonant frequency) [21], [22]. However, it is difficult to identify the accurate linear dynamics for frictional servo systems due to the influence of nonlinear friction.

In regard to FRA methods for frictional systems, many literatures have been presented in recent years, especially on friction model identification. For instance, the references [20]−[26] addressed the frequency-domain identification procedures and/or their effectiveness for simple static friction models, LuGre models, and elasto-plasticity models. On the other hand, some research works presented FRA methods to identify the linear dynamics. The traditional and simple way to obtain the correct linear dynamics is to apply larger excitation force in a sine sweep experiment so that effective excitation thrust for the linear dynamics becomes much larger than friction [10], [26]. However, the larger excitation amplitude is often restricted because of mechanical noises and damages, input saturation in servo amplifiers, etc. By contrast, the reference [27] most closely related to this study examined a friction model-based FRA method identifying the linear dynamics. The FRA concept is to compensate for nonlinear friction, which allows to achieve an FRA result of the correct linear dynamics with smaller excitation force. However, since the FRA approach does not consider phase delay properties in a current control system, sensor signal transfer and transportation, etc., which actually exist in the plant system, it would cause identification errors for the linear dynamics as well as deterioration of system stability. Furthermore, the aforementioned literatures concerning FRA for frictional systems did not discuss FRA results for resonant modes in higher frequencies, which would be important knowledge to related research fields of the fast and precise motion control.

In this study, an advanced friction model-based FRA method considering phase delay properties is presented to identify a precise linear plant model for effective controller design and accurate system analyses. The proposed FRA has simple structure with the friction model and the phase delay model, and is constructed by using the friction model-based effective thrust observer (no friction compensation) [28]. The theoretical advantages are clarified in detail, in comparison to two conventional FRA methods: one is a traditional FRA without a

Y. Maeda and M. Iwasaki are with Department of Electrical and Mechanical Engineering, Nagoya Institute of Technology, Gokiso, Showa, Nagoya 4668555, Japan (e-mail: ymaeda@nitech.ac.jp).

Manuscript received July 31, 2017; revised Jan. 13, 2018.

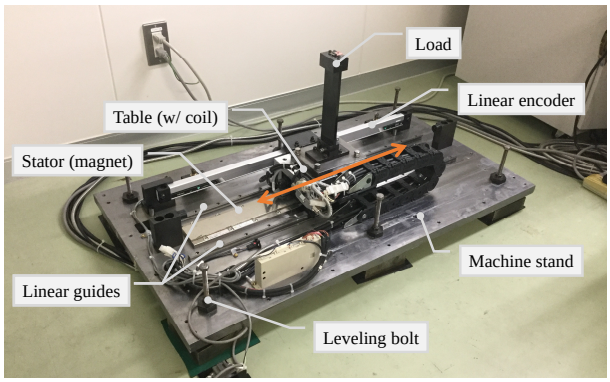

Fig. 1. Linear-motor-driven table, as laboratory prototype.

TABLE I
DIMENSIONS OF TABLE MECHANISM.

Table (w/ coil)	
Size	$176 \times 202 \times 54$ mm
Weight	6.0 kg
Mass load	
Weight	2.5 kg
Machine stand	
Size	$560 \times 1000 \times 25$ mm
Weight	110 kg
Linear motor (Sanyo Denki, DS050)	
Effective stroke	780 mm
Rated speed	2.0 m/s
Rated thrust	150 N
Linear encoder (Mitutoyo, AT211)	
Effective range	800 mm
Resolution	0.1 μm

friction model [25] which is widely used in industry because of simplicity, and the other is a friction model-based FRA without consideration of phase delay properties [27] which has the add-on structure for the traditional FRA. In addition, influence of the modeling error on the phase delay model is examined in order to demonstrate the reliability of the proposed FRA. On the other hand, as a case study, the proposed FRA is applied to the linear plant model-based feedfoward (FF) control design [9] for the fast and precise positioning control, where the FRA accuracy is comparatively evaluated. The effectiveness of the proposed FRA is demonstrated through theoretical analyses and experiments for a laboratory prototype linear-motor-driven table system.

II. Influence of Nonlinear Friction on Frequency Response Analysis

A. Linear-Motor-driven Table

Fig. 1 shows a laboratory prototype of table positioning system, while Table I lists dimensions of the table mechanism. The target servo system is an imitation device of typical industrial servo mechanisms in electronics manufacturing machines, machine tools, etc. A moving table on a machine stand is driven by a moving-magnet-type AC linear motor along two linear guides using rolling ball mechanisms. The machine stand is supported by six leveling bolts on the floor, while a mass load is mounted on the table through a

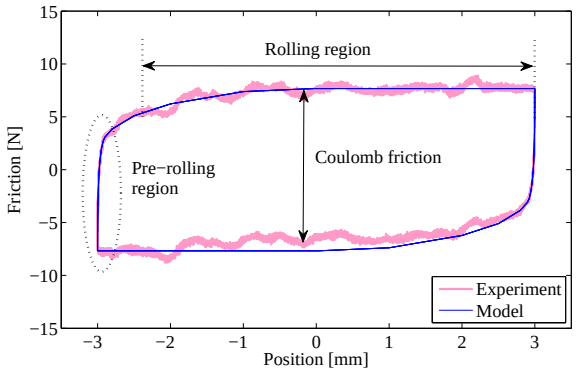

(a) Overall view

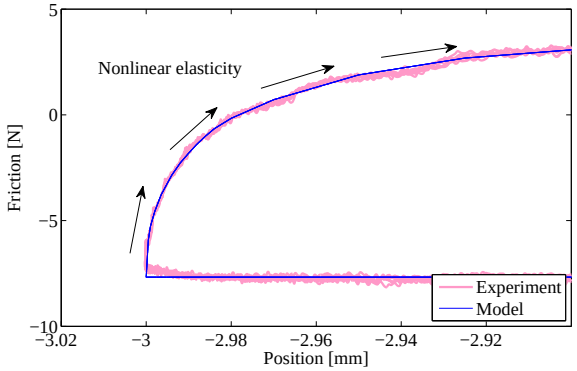

(b) Close-up view of pre-rolling region

Fig. 2. Nonlinear elastic characteristics of rolling friction.

flexible beam. High-acceleration positioning motion excites mechanical resonant vibrations of the machine stand and the flexible load, which deteriorate the table positioning accuracy. In addition, nonlinear friction (rolling friction) exists at the contact points between the rolling elements and the guides with lubricant grease, where its nonlinear phenomena make it complicated to analyze system behavior and to design effective controllers. The table position is detected by a linear encoder, and is controlled in a full-closed position control manner through a DSP (SDS, PCI-DSP46713, sampling time of 500 μs) and an AC servo amplifier (Sanyo Denki, PY0). The servo amplifier controls the motor current with its control bandwidth of about 750 Hz.

B. Nonlinear Friction Characteristic

Light lines in Fig. 2 indicate rolling friction characteristics measured by moving the table with a low-frequency sinusoidal position trajectory (frequency of 0.05 Hz). Fig. 2(a) shows an overall view of the hysteresis property, while Fig. 2(b) shows a close-up view of the pre-rolling region, respectively. The rolling friction generates constant Coulomb friction (about 7.7 N) in the rolling region (macro-displacement region). In the pre-rolling region (micro-displacement region), on the other hand, the rolling friction shows nonlinear elastic behavior depending on displacement. In particular, the friction force drastically varies in the displacement region of less than 100 μm after the velocity reversal as shown in Fig. 2(b). In addition, the hysteresis curve dynamically varies depending

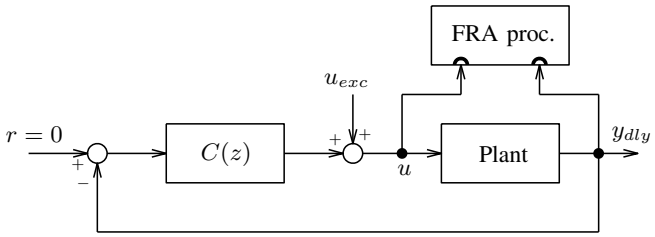

Fig. 3. Block diagram of traditional FRA method (Conventional FRA-1).

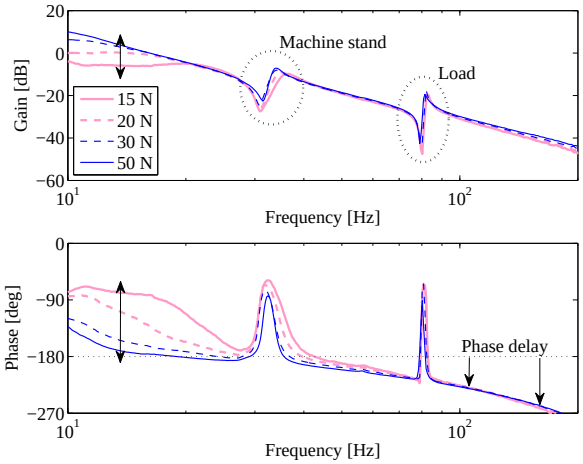

Fig. 4. Bode plots of plant system in different excitation amplitude.

on history of the past position trajectory (so-called "history dependency" or "memory characteristic") [12], [14].

C. Frequency Characteristic

Fig. 3 shows a block diagram of a feedback (FB) control system and an FRA system with a sine sweep ("Conventional FRA-1" defined later), which is widely used by industrial engineers. Here, "Plant" is the target plant system, $C(z)$ is the FB controller, r is the target position, y_{dly} is the plant output corresponding to the detected table position, u is the control input corresponding to the motor thrust reference, and u_{exc} is the sinusoidal signal for excitation defined as $u_{exc}(t) = A_{exc} \sin 2\pi f_{exc} t$, respectively. In the sine sweep experiment, f_{exc} is sequentially increased from 10 Hz to 200 Hz (total number of excitation frequencies is 400), and the time-domain signals of u and y_{dly} are transformed to the frequency-domain signals based on the Discrete Fourier Transform (DFT). The FRA processing is performed by a servo analyzer (Ono Sokki, DS-3200).

Fig. 4 shows experimental FRA results, where A_{exc} is selected as $15, 20, 30$, and 50 N to clarify influence of the nonlinearity in the rolling friction. From the figure, each FRA result shows quite different frequency characteristics depending on the excitation amplitude, i.e., gain and phase in the low frequency range less than 20 Hz, the primary resonant mode around 34 Hz (due to the machine stand), and the second resonant mode around 82 Hz (due to the flexible load). Such remarkable changes, especially in the low frequency range, are well-known phenomena due to the nonlinear elasticity of the rolling friction [12], [25]−[27]. In order to prevent the influence of nonlinearity in frequency-domain identification, increase of the excitation amplitude is a traditional and effective way. However, sufficiently-large excitation is restricted because of physical saturation of amplifiers and mechanical noises and damages. On the other hand, there exists a phase delay property in the high frequency range, which is caused by the D/A conversion of the DSP, the current control system and the low-pass filters in the servo amplifier, and the transfer delay of the encoder signal to the DSP through the servo amplifier.

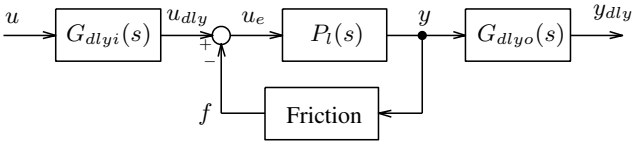

Fig. 5. Conceptual block diagram of plant system with friction and phase delays.

A conceptual block diagram of a general frictional plant system is expressed by Fig. 5 in continuous-time domain, with a linear mechanical dynamics, two phase delay properties, and nonlinear friction. In the figure, $P_l(s)$ is the linear dynamics, $G_{dlyi}(s)$ and $G_{dlyo}(s)$ are the phase delay properties on input and output, "Friction" is the nonlinear friction as a function of position, u_e is the effective thrust for $P_l(s)$, u_{dly} is the motor thrust after $G_{dlyi}(s)$, y is the table position before $G_{dlyo}(s)$, and f is the nonlinear friction, respectively. $P_l(s)$ is defined as (1), considering the rigid mode and the two resonant modes:

$$P_l(s) = \frac{y(s)}{u_e(s)} = \frac{k_0}{s^2} + \sum_{j=1}^{2} \frac{k_j}{s^2 + 2\zeta_j \omega_j s + \omega_j^2}, \qquad (1)$$

where k_0 is the rigid mode gain, k_j is the vibration mode gain of the j-th vibration mode, $\omega_j (= 2\pi f_j)$ is the resonant angular frequency, and ζ_j is the damping coefficient, respectively. In order to realize the fast and precise positioning motion without vibratory response due to the resonant modes, the correct FRA result for the linear mechanical dynamics of (1) is required not only in the low frequency range but also around the resonant frequencies.

III. Theoretical Examinations of Friction Model-Based FRA for Frictional System with Phase Delays

Principles of the following three FRA methods are theoretically examined in detail, for the frictional system with phase delays defined by Fig. 5.

- Conventional FRA-1: a traditional FRA method introduced in II-C [25] as the most popular FRA method in industry.
- Conventional FRA-2: an FRA method performing friction compensation through a friction model with the add-on structure for Conventional FRA-1 [27].
- Proposed FRA: an FRA method estimating the effective thrust with a friction model and a phase delay model.

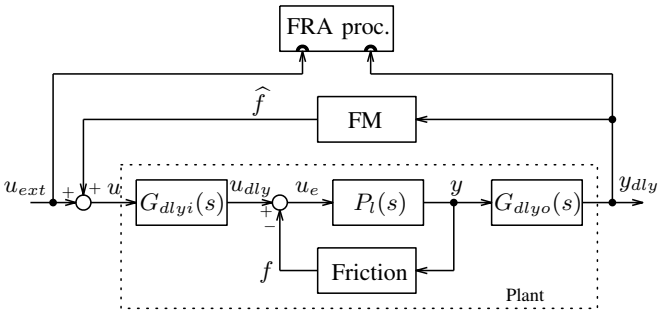

Fig. 6. Block diagram of Conventional FRA-2.

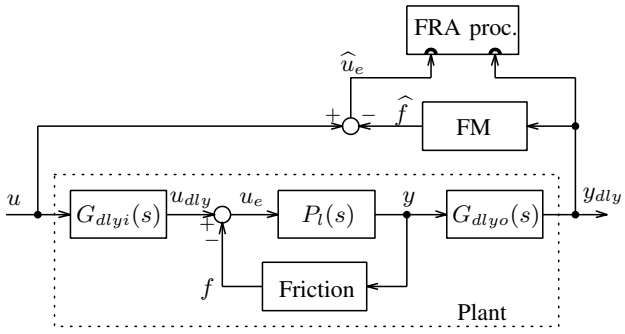

Fig. 7. Equivalent diagram of Conventional FRA-2 as observer-type.

A. Conventional FRA-1

The general FRA system shown in Fig. 3 uses the control input u and the detected table position y_{dly} as input and output in order to analyze the linear dynamics $P_l(s)$ (i.e., the FRA result $\widehat{P}_l(j\omega)$ of Conventional FRA-1 is $y_{dly}(j\omega)/u(j\omega)$). However, as is clear from (1) and Fig. 5, the actual input and output of $P_l(s)$ are respectively u_e and y. Since u and y_{dly} as inputs to the FRA processing are respectively defined as $u(s) = G_{dlyi}^{-1}(s)\{u_e(s) + f(s)\}$ and $y_{dly}(s) = G_{dlyo}(s)y(s)$ by using u_e, y, and f, the transfer characteristic of y_{dly} from u is formulated as follows:

$$\frac{y_{dly}(s)}{u(s)} = \frac{G_{dlyo}(s)y(s)}{G_{dlyi}^{-1}(s)\{u_e(s) + f(s)\}}. \tag{2}$$

By assuming $G_{dlyi}(s) \simeq 1$ and $G_{dlyo}(s) \simeq 1$ (no phase delay) for simplicity, (2) can be transformed as

$$\frac{y_{dly}(s)}{u(s)} \simeq \frac{y(s)}{u_e(s) + f(s)}. \tag{3}$$

From (3), if $f(s) \neq 0$, then this FRA method cannot identify $P_l(s)$ essentially. Therefore, larger excitation signals satisfying $|u_e(s)| \gg |f(s)|$ are required to obtain an accurate FRA result for the linear dynamics [12], [14], [25], [26].

B. Conventional FRA-2

The reference [27] presents a friction model-based FRA method with consideration of the issue in Conventional FRA-1. Fig. 6 shows a block diagram of Conventional FRA-2, where "FM" is the friction model for estimate of f by using y_{dly}. Here, FM should be prepared before performing FRA. In Conventional FRA-2, the estimated friction $\widehat{f}$ is added to the control input u as a FB compensation to cancel f, and the extended control input u_{ext} and y_{dly} are transfered to the FRA processing (i.e., the FRA result $\widehat{P}_l(j\omega)$ of Conventional FRA-2 is $y_{dly}(j\omega)/u_{ext}(j\omega)$). The transfer characteristic of y_{dly} from u_{ext} is expressed as follows, by using u_e, y, f, and $\widehat{f}$:

$$\begin{aligned}\frac{y_{dly}(s)}{u_{ext}(s)} &= \frac{G_{dlyo}(s)y(s)}{G_{dlyi}^{-1}(s)\{u_e(s) + f(s)\} - \widehat{f}} \\ &= \frac{G_{dlyi}(s)G_{dlyo}(s)y(s)}{u_e(s) + f(s) - G_{dlyi}(s)\widehat{f}}.\end{aligned} \tag{4}$$

Here, since the denominator of right hand side of (4) includes the term of $\widehat{f}$, it is assumed to satisfy $\widehat{f} = G_{dlyo}(s)f$ by using a precise FM. In such case, (4) is formulated as (5) by using u_e, y, and f.

$$\frac{y_{dly}(s)}{u_{ext}(s)} = \frac{G_{dlyi}(s)G_{dlyo}(s)y(s)}{u_e(s) + \{1 - G_{dlyi}(s)G_{dlyo}(s)\}f(s)} \tag{5}$$

If $G_{dlyi}(s) \simeq 1$ and $G_{dlyo}(s) \simeq 1$ (no phase delay), then (5) is expressed as

$$\frac{y_{dly}(s)}{u_{ext}(s)} \simeq \frac{y(s)}{u_e(s)} = P_l(s). \tag{6}$$

Hence, Conventional FRA-2 can obtain the accurate FRA result $\widehat{P}_l(j\omega)$, if there is no phase delay property in the plant. However, since the plant system actually includes the phase delay properties (i.e., $G_{dlyi}(s) \neq 1$ and $G_{dlyo}(s) \neq 1$), Conventional FRA-2 also cannot estimate the correct information of $P_l(s)$ from the FRA result in principle, as expressed by (5). In addition, the FB friction compensation error due to the phase delay may cause deterioration of system stability during the sine sweep.

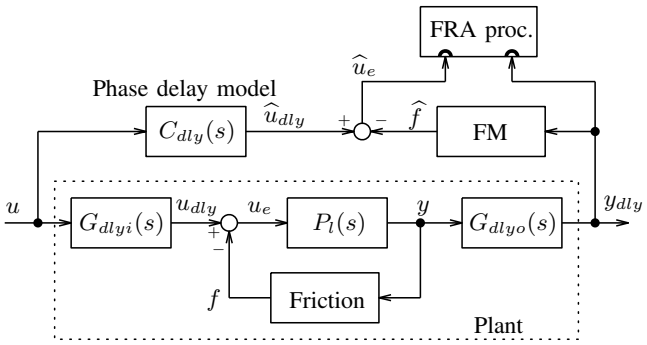

Fig. 8. Block diagram of Proposed FRA.

C. Proposed FRA

Considering the subject issues in the conventional FRA approaches in III-A and III-B, Proposed FRA is constructed as an observer-type for u_e. Fig. 7 shows an equivalent block diagram of Conventional FRA-2 as the observer-type construction, where $\widehat{u}_e$ is the estimated effective thrust which is calculated by using u and $\widehat{f}$, and is transfered to the FRA processing (i.e., the FRA result $\widehat{P}_l(j\omega)$ is $y_{dly}(j\omega)/\widehat{u}_e(j\omega)$). Since $\widehat{f}$ estimated by FM is not fed back to the control loop, the observer-type construction does not suffer from

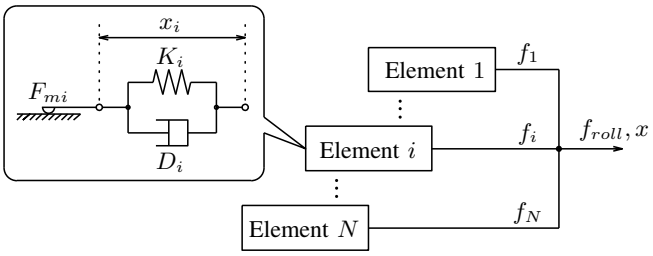

Fig. 9. Conceptual diagram of rolling friction model.

the stability deterioration. With the assumption of $\widehat{f}(s) = G_{dlyo}(s)f(s)$, the transfer characteristic of y_{dly} from $\widehat{u}_e$ in Fig. 7 is defined as (7) by using u_e, y and f.

$$\frac{y_{dly}(s)}{\widehat{u}_e(s)} = \frac{G_{dlyi}(s)G_{dlyo}(s)y(s)}{u_e(s) + \{1 - G_{dlyi}(s)G_{dlyo}(s)\}f(s)} \tag{7}$$

It is obvious that right hand side of (7) is still affected by $G_{dlyi}(s)$ and $G_{dlyo}(s)$ and is equivalent to the ones of (2) and (5).

Fig. 8 shows a block diagram of Proposed FRA, where the FRA result $\widehat{P}_l(j\omega)$ is defined as $y_{dly}(j\omega)/\widehat{u}_e(j\omega)$. Proposed FRA is composed of FM and a phase delay model $C_{dly}(s)$ as Smith compensation. Note here that FM as well as $C_{dly}(s)$ should be constructed in advance. By introducing $C_{dly}(s)$ on the path of u for estimation of the delayed motor thrust $\widehat{u}_{dly}$, $\widehat{u}_e$ is expressed as (8) as a function of u_e and f with consideration of $u(s) = G_{dlyi}^{-1}(s)\{u_e(s) + f(s)\}$ and $\widehat{f}(s) = G_{dlyo}(s)f(s)$:

$$\begin{aligned}\widehat{u}_e(s) &= \widehat{u}_{dly}(s) - \widehat{f}(s) \\ &= C_{dly}(s)G_{dlyi}^{-1}(s)\{u_e(s) + f(s)\} - G_{dlyo}(s)f(s). \end{aligned}\tag{8}$$

If $C_{dly}(s) = G_{dlyi}(s)G_{dlyo}(s)$ is satisfied, then (8) can be transformed as

$$\widehat{u}_e(s) = G_{dlyo}(s)u_e(s). \tag{9}$$

Therefore, the transfer characteristic of y_{dly} from $\widehat{u}_e$ can satisfy the following equation.

$$\frac{y_{dly}(s)}{\widehat{u}_e(s)} = \frac{G_{dlyo}(s)y(s)}{G_{dlyo}(s)u_e(s)} = \frac{y(s)}{u_e(s)} = P_l(s) \tag{10}$$

It is clear that although $\widehat{f}$ is delayed by $G_{dlyo}(s)$ to f, $C_{dly}(s)$ synchronizes the time axis of $\widehat{u}_e$ with $\widehat{f}$. As a result, Proposed FRA can obtain the accurate information of $P_l(s)$ even if the phase delay properties exist in the plant. Note that, in the design of $C_{dly}(s)$, it is unnecessary to distribute $C_{dly}(s)$ to $G_{dlyi}(s)$ and $G_{dlyo}(s)$, since the information of only phase difference between u and y_{dly} is needed to realize (10).

IV. Design Procedure of Proposed FRA

A. Friction Model

Various kinds of friction models and their parameter identification techniques, e.g., LuGre model [25], elasto-plastic model [26], Leuvan model [20], and GMS model [12], [13], have been presented in literatures, while the effective and widespread friction models are available in the friction model-based FRA. In this study, a multi-structure friction model [14], [15] such as GMS model, which considers rheological phenomena at contact points of friction surface, is introduced as a case study, since the multi-structure model has an advantage in expression of the memory characteristic of rolling friction. Fig. 9 shows a conceptual diagram of the rolling friction model with N elementary models in parallel. Each elementary model ($i = 1, \ldots, N$) is defined as follows:

TABLE II
Parameters of rolling friction model.

Element i	F_{mi} [N]	K_i [N/mm]	D_i [Ns/mm]
1	1.12	2226.6	0.0
2	0.60	602.1	0.0
3	0.33	165.1	0.0
4	0.54	154.9	0.0
5	0.49	81.6	0.0
6	0.46	56.8	0.0
7	0.16	15.8	0.0
8	0.36	30.0	0.0
9	0.25	17.9	0.0
10	0.73	45.8	0.0
11	0.73	36.2	0.0
12	0.88	29.3	0.0
13	1.34	26.8	0.0
14	1.23	16.4	0.0
15	0.77	7.7	0.0
16	0.72	3.6	0.0
17	0.97	2.0	0.0
18	1.08	1.1	0.0
19	1.74	0.9	0.0
20	0.89	0.3	0.01

$$x_i = \begin{cases} x + x_{ri} & (|x_i| < X_{mi}) : \text{ stick} \\ \text{sgn}(\frac{dx}{dt})X_{mi} & (|x_i| = X_{mi}) : \text{ slip} \end{cases}, \tag{11}$$

$$f_i = K_i x_i + D_i \frac{dx_i}{dt}, \tag{12}$$

$$F_{mi} = K_i X_{mi}, \tag{13}$$

$$-X_{mi} \le x_i \le X_{mi}, \quad -F_{mi} \le f_i \le F_{mi}, \tag{14}$$

where x is the displacement input corresponding to the detected table position y_{dly}, x_i is the element displacement, x_{ri} is the element displacement at velocity reversal, f_i is the element force, X_{mi} is the maximum element displacement, F_{mi} is the maximum element force, K_i is the element elastic coefficient, D_i is the element viscous coefficient, and $\text{sgn}(\cdot)$ is the sign function, respectively. The elementary model generates viscoelastic friction force in the stick region and the static force with the limit stress of $\pm F_{mi}$ in the slip region. The rolling friction force f_{roll} is calculated as follows, by using N elementary models' outputs:

$$f_{roll} = \sum_{i=1}^{N} f_i. \tag{15}$$

The number of elements N is selected as $N = 20$ with consideration of the model accuracy, while the parameters, K_i, D_i, and F_{mi}, are identified as listed in Table II, according to the Back Propagation algorithm for the measured hysteresis characteristic shown in Fig. 2 [15]. Note here that $N \ge 8$ was sufficient for the target table system, in terms of the evaluation value of the Back Propagation algorithm. Dark solid lines in

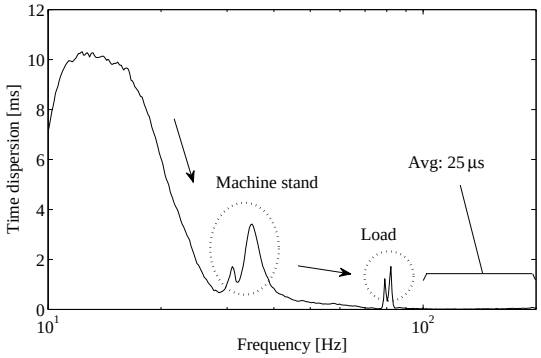

Fig. 10. Frequency characteristic of phase dispersion of $y_{dly}(j\omega)/u(j\omega)$.

Fig. 2 indicate the model characteristics, where the model reproduces the actual nonlinear properties.

On the other hand, in order to compensate for the viscosity of friction, the following simple viscous friction model is additionally introduced:

$$f_{vis} = D_v v, \tag{16}$$

where f_{vis} is the viscous friction force, v is the table velocity corresponding to dy_{dly}/dt, and D_v is the viscous friction coefficient, respectively. D_v was identified as $D_v = 0.00235$ Ns/mm by constant velocity drive experiments [10].

Finally, the friction model FM in Fig. 8 is formulated by (11)∼(16) and its output is calculated as

$$\widehat{f} = f_{roll} + f_{vis}. \tag{17}$$

B. Phase Delay Model

In this study, the phase delay property existing in the actual plant system is simply modeled as an equivalent delay time component, following the procedures below.

1) A sine sweep experiment is performed and a phase plot $\phi(j\omega)$ of $y_{dly}(j\omega)/u(j\omega)$ is obtained by using Conventional FRA-1 (traditional way).
2) A phase delay ϕ_L at a high frequency f_L is selected from $\phi(j\omega)$.
3) The equivalent delay time L is calculated with ϕ_L and f_L.

In the first step 1), it is sufficient to obtain only one experimental result with small excitation force, since influence of the excitation force is obviously small in the high frequency range over 100 Hz. In order to clarify the above explanation, Fig. 10 shows the phase dispersion from the averaged phase $\phi_{avg}(j\omega)$ which is calculated by using $\phi(j\omega)$ (four excitation cases) depicted in Fig. 4. Notice here that the dispersion at the frequency of f_{exc} is expressed in the time domain as $\max\{|\phi_{avg}(j2\pi f_{exc}) - \phi(j2\pi f_{exc})|/360 f_{exc}\}$. From the figure, the dispersion tends to reduce at higher frequencies over 100 Hz, where the averaged dispersion is only 25 μs.

In the second step 2), only a frequency f_L for estimate of L is selected from the high frequency range where high-order resonant modes do not appear, considering the phase dispersion shown in Fig. 10.

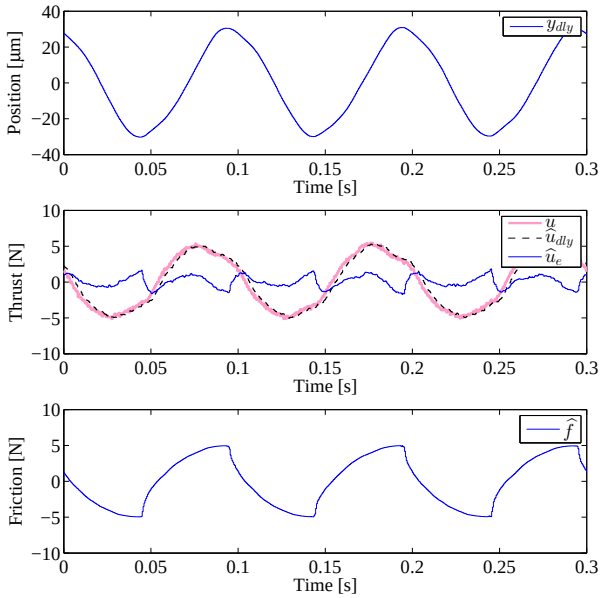

Fig. 11. Experimental response waveforms at excitation frequency of 10 Hz in Proposed FRA.

In the third step 3), L can be calculated by the following equation:

$$L = \frac{-180 - \phi_L}{360 f_L}, \tag{18}$$

where the phase of $P_l(s)$ is assumed as -180 deg in the high frequency range since $P_l(s)$ includes a rigid mode as (1).

By using L identified through the above procedures, $C_{dly}(s)$ in Fig. 8 is mathematically formulated as follows, according to the fourth-order Pade approximation:

$$C_{dly}(s) = \frac{(Ls)^4 - 20(Ls)^3 + 180(Ls)^2 - 840Ls + 1680}{(Ls)^4 + 20(Ls)^3 + 180(Ls)^2 + 840Ls + 1680}. \tag{19}$$

In this study, the phase plot measured by the smallest excitation amplitude of $A_{exc} = 15$ N (depicted by the light solid line in Fig. 4) was used for identification of L, while L was identified as $L = 1.38$ ms at $f_L = 120$ Hz at random. Note that the other identification approaches and mathematical models are available in the design of $C_{dly}(s)$.

V. Experimental Evaluations

A. Frequency Response Analysis

In order to verify advantages of Proposed FRA which are theoretically examined in III, FRA experiments are performed in comparison with Conventional FRA-1 and Conventional FRA-2. Estimation of $\widehat{u}_e$ is performed in a DSP (dSPACE, DS1104, sampling time of 500 μs) online, where FM of (11)∼(17) and $C_{dly}(s)$ of (19) are discretized for implementation. Conventional FRA-2 is constructed as the observer-type of Fig. 7, where the same friction model FM as of Proposed FRA is used. In the following experimental evaluations, the excitation signal of $A_{exc} = 15$ N (the smallest case in Fig. 4) is used in all the FRA methods, supposing

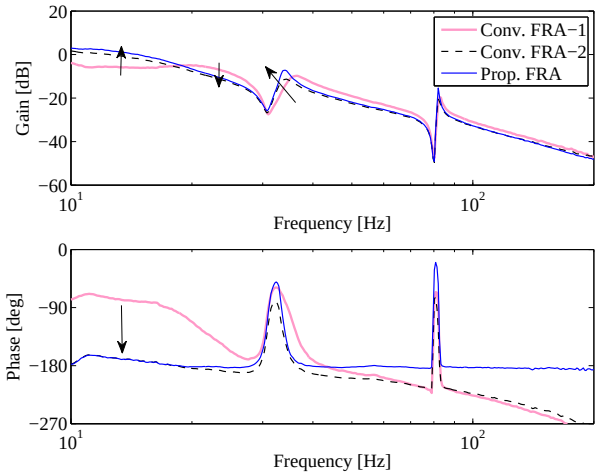

Fig. 12. Comparison of FRA results $\widehat{P}_l(j\omega)$ with excitation amplitude of $A_{exc} = 15$ N.

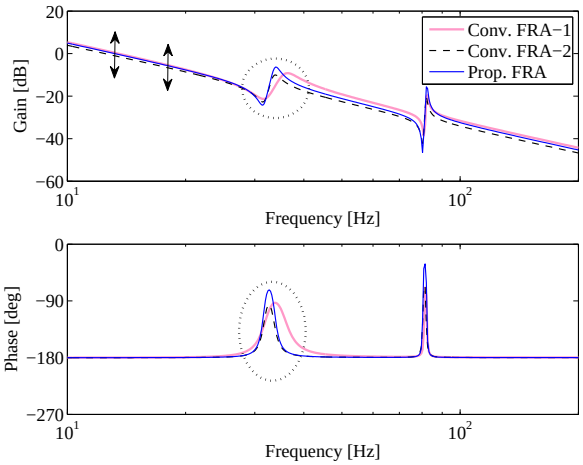

Fig. 13. Comparison of identified linear plant dynamics $\widehat{P}_l(s)$.

the saturation of the control input and the mechanical noises/damages. Here, since Proposed FRA and Conventional FRA-2 estimate $\widehat{f}$ by using the detected position y_{dly}, accuracy (resolution) of the position sensor should be carefully considered. It is recommended to use high resolution position sensors or to apply smoothing processing to low resolution signals in order to conduct the accurate FRA. In this study, the resolution of 0.1 μm of the linear encoder was enough for the target table system.

First, Fig. 11 shows an example of time response waveforms of the detected table position y_{dly}, the motor thrust u as the control input, the estimated motor thrust with the phase delay $\widehat{u}_{dly}$, the estimated effective thrust $\widehat{u}_e$, and the estimated friction $\widehat{f}$, at the excitation frequency of $f_{exc} = 10$ Hz. From Fig. 11, Proposed FRA estimates $\widehat{u}_e$ for the FRA processing from the original signals u and y_{dly}. In Conventional FRA-1 and Conventional FRA-2, the influence of the nonlinear friction or the phase delay property are not considered.

Next, Fig. 12 shows comparative FRA results $\widehat{P}_l(j\omega)$ by three FRA methods. In comparison to Conventional FRA-1 indicated by light solid lines, Conventional FRA-2 of dark broken lines shows the gain increase and the phase delay in the low frequency range under 20 Hz, which shows similar characteristic with that of Conventional FRA-1 with the larger excitation force as shown in Fig. 4. Notice here, in both conventional FRA methods, the FRA results show the remarkable phase delays in the high frequency range, since they cannot estimate the linear plant dynamics $P_l(s)$ of (1) theoretically as explained in III-A and III-B. On the other hand, Proposed FRA obtains the further gain increase in the low frequency range in comparison to Conventional FRA-2 and prevent the phase delay property in the high frequency range, which are considered as influence of the phase delay compensation. In addition, in the cases of Proposed FRA and Conventional FRA-2, the primary resonant characteristics around 34 Hz are varied compared to Conventional FRA-1. The difference is expected as influence of the friction estimation.

TABLE III
IDENTIFIED PARAMETERS OF $\widehat{P}_l(s)$.

Parameter	Unit	Conv. FRA-1	Conv. FRA-2	Prop. FRA
k_0	mm/Ns^2	99.74	83.32	94.28
k_1	mm/Ns^2	23.90	9.07	13.08
f_1	rad/s	35.68	33.45	33.32
ζ_1	($\times 10^{-2}$)	6.01	2.96	2.48
k_2	mm/Ns^2	3.60	3.46	5.27
f_2	rad/s	82.20	81.85	82.22
ζ_2	($\times 10^{-3}$)	4.17	5.22	3.22

Fig. 13 indicates bode plots of identified linear plant model $\widehat{P}_l(s)$ for each FRA result in Fig. 12, by applying the differential iterative method to the parameter identification. The target frequency range for identification is chosen as $20 \sim 200$ Hz to omit the influence of the nonlinear friction in the low frequency range. In addition, the phase delays in the high frequency range of Conventional FRA-1 and Conventional FRA-2 shown in Fig. 12 are corrected by using a delay model such as $e^{-L_c s}$ (L_c is the delay time for correction) in advance so that the corrected phases become around -180 deg in the high frequency range. Table III lists a comparison of the identified parameters. From Fig. 13 and Table III, since the FRA results are different each other, the obtained models have different frequency characteristics owing to the rigid mode gain k_0 and the primary resonant mode parameters k_1, f_1, and ζ_1.

B. Influence of Phase Delay Model Error on Proposed FRA

In order to demonstrate the reliability of Proposed FRA for the error in the phase delay model $C_{dly}(s)$, an experiment which gives the incorrect delay time L_e using the delay time error ΔL (i.e., $L_e = L - \Delta L$) instead of L in (19) was conducted (influence of the friction model error has been discussed in detail in the reference [28]). Fig. 14 shows experimental results of $\widehat{P}_{le}(j\omega)/\widehat{P}_l(j\omega)$, where $\widehat{P}_l(j\omega)$ is the reference FRA result with $L = 1.38$ ms indicated by the dark solid lines in Fig. 12 and $\widehat{P}_{le}(j\omega)$ is the FRA result with ΔL of $25, 50, 100$ μs, and 1.38 ms (equivalent to Conv. FRA-2), assuming the identification error in the high frequency

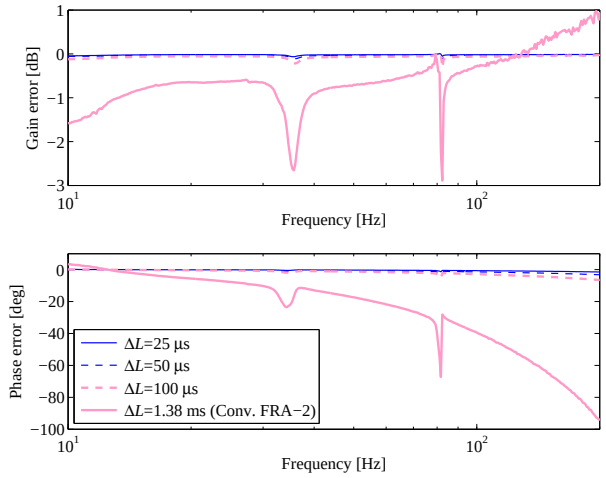

Fig. 14. Bode plots of FRA error $\widehat{P}_{le}(j\omega)/\widehat{P}_l(j\omega)$ on Proposed FRA with phase delay model error.

range as explained in IV-B. From the experimental results of $\Delta L = 25, 50, 100$ μs in Fig. 14, influence of some percent of phase delay error on the FRA accuracy are slight (almost 0 dB in gain and 0 deg in phase) in all frequencies, in comparison to the result of Conventional FRA-2 indicated by light solid lines.

C. Application to Feedforward Control Design

In order to examine the effectiveness of Proposed FRA method aiming at achievement of the accurate linear plant model, the three models shown in Fig. 13 are applied to the model-based feedforward (FF) controller design [9]. Note that Proposed FRA can be applied to various linear plant model-based FF control techniques (e.g., zero phase error tracking control [29], perfect tracking control [7], [30], and final-state control [8], [31]), although the deadbeat FF control [9] is handled in this case study.

Fig. 15 shows a block diagram of the 2DoF table position control system, where $F_r(z)$ and $F_u(z)$ are the FF controllers based on the deadbeat control [9] with $\widehat{P}_l(s)$ as the design model, $C_{dly}(z)$ is the phase delay model of (19) for compensation, $C(z)$ is the PID controller, FM is the friction model composed of (17) for compensation [13], [21], [32], r is the target table position (step signal), r^* is the table position trajectory reference, and u_{ff} is the FF motor thrust, respectively. In this study, the target positioning specification is specified for the position stroke of $r = 0.5$ mm, where y_{dly} should follow r with the settling accuracy of ± 5 μm by the settling time of 50 ms. Note that the same FM, $C_{dly}(z)$, and $C(z)$ are used in all the cases for the fair comparisons. In this 2DoF control system, FM aims at canceling the friction in the positioning, while $F_r(z)$ and $F_u(z)$ mainly determine the position tracking performance as well as the vibration suppression capability. $F_r(z)$ and $F_u(z)$ are designed so that r^* settles to r by 50 ms (see the reference [9] for details). Fig. 16 shows comparative gain characteristics of $F_u(z)$. As can be seen, the gains less than 20 Hz and at the primary resonant mode around 34 Hz are slightly different owing to the

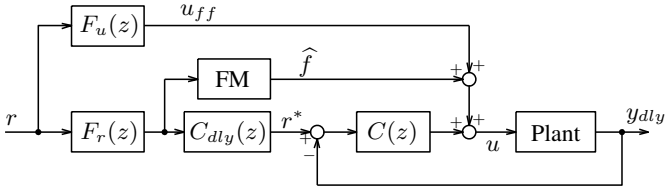

Fig. 15. Block diagram of position control system.

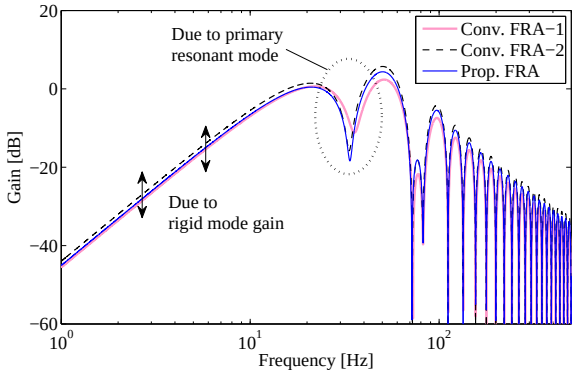

Fig. 16. Gain characteristics of $F_u(z)$.

identified parameters listed in Table III. In the ideal condition, $r^* = y_{dly}$ can be realized according to the model-matching scheme. Therefore, $\widehat{P}_l(s)$ for the FF compensation design should precisely represent the actual frequency characteristic of $P_l(s)$, and the accuracy of $\widehat{P}_l(s)$ is evaluated by the position tracking error $r^* - y_{dly}$.

Fig. 17 shows experimental response waveforms of the position y_{dly}, the position error $r - y_{dly}$, and the position tracking error $r^* - y_{dly}$. In the case of Conventional FRA-1 indicated by light solid lines, the remarkable vibratory response with the frequency of about 34 Hz occurs during the transient and remains at the settling after 50 ms. The reason of the unfavorable vibratory response is expected as the identification error for the primary resonant mode. On the other hand, in comparison to the Conventional FRA-1, Proposed FRA and Conventional FRA-2 suppress the resonant vibration during the positioning motion, by introducing the friction model-based FRA approach. Furthermore, Proposed FRA can obtain better transient tracking performance than Conventional FRA-2, which is supposed to be caused by the difference of the gain in the low frequency range as shown in Fig. 12. It is an advantage of considering the phase delay property in the friction model-based FRA. Table IV lists root mean square error (RMSE) of $r^* - y_{dly}$ during 0.3 s from the starting, where Proposed FRA achieves the best tracking performance in the quantitative evaluation.

From the series of the experimental evaluations, Proposed FRA which considers not only the nonlinear friction but also the phase delay property can improve the accuracy of FRA for identification of the linear dynamics in frictional servo systems. Although the FF control design problem is examined in this case study, Proposed FRA can be applied to observer designs (e.g., disturbance observer) [13], [32], analyses of control systems in time and frequency domains [6], etc. In

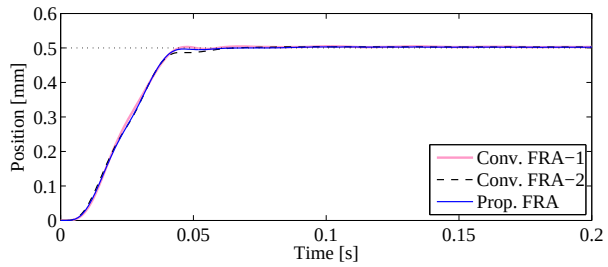

(a) Position

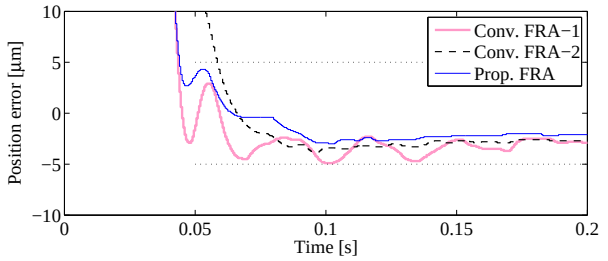

(b) Position error

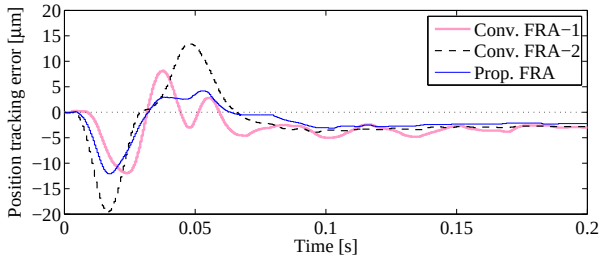

(c) Position tracking error

Fig. 17. Experimental results of fast and precise positioning: (a) position y_{dly}, (b) position error $r - y_{dly}$, and (b) position tracking error $r^* - y_{dly}$.

TABLE IV
COMPARISON OF RMSE.

(Unit: μm)

Conv. FRA-1	Conv. FRA-2	Prop. FRA
2.70	4.55	2.39

addition, the proposed FRA structure which estimates effective thrust can be extended to advanced friction estimation and compensation, by combining the disturbance observer as an example.

VI. CONCLUSION

In this study, an FRA method has been presented to identify the correct linear plant dynamics for frictional servo systems. The proposed FRA has a simple structure with the friction model and the phase delay model, which can estimate effective thrust for the linear dynamics in principle. An example procedure for the proposed FRA system design has been introduced, where the design of the phase delay model has been analytically clarified in detail. By applying the proposed FRA to a table positioning device with nonlinear friction, an improved FRA result could be obtained even if excitation force of the sine sweep was small enough. In addition, influence of the phase delay model error was experimentally investigated. Furthermore, from the fast and precise positioning experiment, the proposed FRA result was sufficiently precise for an effective controller design.

As future works, since the difference in the FRA results still exists between the traditional FRA approach with large excitation force and the proposed FRA, the reason will be investigated to further improve the FRA accuracy, especially by focusing on the nonlinear friction behavior during the sine sweep.

ACKNOWLEDGMENT

This work was supported by The Nitto Foundation, Japan. In addition, the authors would like to thank Via Mechanics, Ltd, for supporting experimental equipment.

REFERENCES

[1] M.-Y. Chen and J.-S. Lu, "High-precision motion control for a linear permanent magnet iron core synchronous motor drive in position platform," *IEEE Trans. Ind. Informat.*, vol. 10, no. 1, pp. 99–108, 2014.
[2] M. Li, Y. Zhu, K. Yang, and C. Hu, "A data-driven variable-gain control strategy for an ultra-precision wafer stage with accelerated iterative parameter tuning," *IEEE Trans. Ind. Informat.*, vol. 11, no. 5, pp. 1179–1189, 2015.
[3] M. Iwasaki, K. Seki, and Y. Maeda, "High-precision motion control techniques: a promising approach to improving motion performance," *IEEE Ind. Electron. Magazine*, vol. 6, no. 1, pp. 32-40, 2012.
[4] K. Seki and M Iwasaki, "Improvement of bending vibration suppression performance for galvano mirror by self-sensing actuation," *IEEJ Jounal Ind. Applications*, vol. 3, no. 1, pp. 10–17, 2014.
[5] Y. Z. Tan and C. K. Pang, "On using Nyquist plots for relaxing convex conservative approximations in design of robust mechatronic systems," in *Proc. 7th IFAC Symposium Mechatron. Syst.*, 2016, pp. 115–119.
[6] T. Atsumi, "Emerging technology for head-positioning system in HDDs," *IEEJ Jounal Ind. Applications*, vol. 5, no. 2, pp. 117–122, 2016.
[7] H. Fujimoto, Y. Hori, and A. Kawamura, "Perfect tracking control based on multirate feedforward control with generalized sampling periods," *IEEE Trans. Ind. Electron.*, vol. 48, no. 3, pp. 636–644, 2001.
[8] M. Hirata, T. Hasegawa, and K. Nonami, "Seek control of hard disk drives based on final-state control taking account of the frequency components and the magnitude of control input," in *Proc. 7th Int. Workshop Advanced Motion Control*, 2002, pp. 40–45.
[9] Y. Maeda and M. Iwasaki, "Improvement of adaptive property by adaptive deadbeat feedforward compensation without convex optimization," *IEEE Trans. Ind. Electron.*, vol. 62, no. 1, pp. 466–474, 2015.
[10] T. Takemura and H. Fujimoto, "Simultaneous identification of linear parameters and nonlinear rolling friction for ball screw driven stage," in *Proc. IEEE 37th Annual Conf. Ind. Electron. Society*, 2011, pp. 3424–3429.
[11] H. Sekine, S. Ueda, and M. Hirata, "System identification of a galvano scanner using input-output data obtained from positioning control," in *Proc. 2015 European Control Conf.*, 2015, pp. 1297–1302.
[12] F. Al-Bender and J. Swevers, "Characterization of friction force dynamics," *IEEE Control Systems Magazine*, vol. 28, no. 6, pp. 64–81, 2008.
[13] Z. Jamaludin, H. Van Brussel, and J. Swevers, "Friction compensation of an XY feed table using friction-model-based feedforward and an inverse-model-based disturbance observer," *IEEE Trans. Ind. Electron.*, vol. 56, no. 10, pp. 3848–3853, 2009.
[14] Y. Maeda and M. Iwasaki, "Rolling friction model-based analyses and compensation for slow settling response in precise positioning," *IEEE Trans. Ind. Electron.*, vol. 60, no. 12, pp. 5841–5853, 2013.
[15] Y. Maeda and M. Iwasaki, "Initial friction compensation using rheology-based rolling friction model in fast and precise positioning," *IEEE Trans. Ind. Electron.*, vol. 60, no. 9, pp. 3865–3876, 2013.
[16] M. Ruderman and M. Iwasaki, "On damping characteristics of frictional hysteresis in pre-sliding range," *IEEE Trans. on Ind. Electron.*, vol. 62, no. 9, pp. 5941–5949, 2015.

[17] T. Beauduin and H. Fujimoto, "Distributed and parameter-varying friction compensation for ball-screw feed drive systems," in *Proc. 2017 IEEJ Int. Workshop Sensing, Actuation, Motion Control, and Optimization*, 2017, IS1-3.
[18] T. Koizumi and H. Shibazaki, "A study on the relationships governing starting rolling friction," *Wear*, vol. 93, pp. 281–290, 1984.
[19] S. Futami, A. Furutani, and S. Yoshida, "Nanometer positioning and its micro-dynamics," *Nanotechnology*, vol. 1, no. 1, pp. 31–37, 1990.
[20] V. Lampaert, J. Swevers, and J. De Schutter, "Impact of nonlinear friction on frequency response function measurements," in *Proc. Int. Conf. Noise and Vibration Eng.*, 2000, pp. 443–450.
[21] Z. Chen, B. Yao, and Q. Wang, "Adaptive robust precision motion control of linear motors with integrated compensation of nonlinearities and bearing flexible modes," *IEEE Trans. Ind. Informat.*, vol. 9, no. 2, pp. 4453–4458, 2013.
[22] Q. Xu, "Design and smooth position/force switching control of a miniature gripper for automated microhandling," *IEEE Trans. Ind. Informat.*, vol. 10, no. 2, pp. 1023–1032, 2014.
[23] S.-J. Kim and I.-J. Hz, "A frequency-domain approach to identification of mechanical systems with friction," *IEEE Trans. Automatic Control*, vol. 46, no. 6, pp. 888–893, 2001.
[24] Y.-Y. Chen, P.-Y. Huang, and J.-Y. Yen, "Frequency-domain identification algorithms for servo systems with friction," *IEEE Trans. Control Syst. Tech.*, vol. 10, no. 5, pp. 654–665, 2002.
[25] R. H. A. Hensen, M. J. G. van de Molengraft, and M. Steinbuch, "Frequency domain identification of dynamic friction model parameters," *IEEE Trans. Control Syst. Tech.*, vol. 10, no. 2, pp. 191–196, 2002.
[26] M. Ruderman and T. Bertram, "FRF based identification of dynamic friction using two-state friction model with elasto-plasticity," in *Proc. 2011 IEEE Int. Conf. Mechatron.*, 2011, pp. 230–235.
[27] C. Li, B. Yao, and X. Zhu, "Analysis and compensation of nonlinear friction effect on frequency identification," in *Proc. 41st Annu. Conf. IEEE Ind. Electron. Society*, 2015, pp. 4453–4458.
[28] Y. Sugiura, J. Kato, Y. Maeda, and M. Iwasaki, "A study on frequency response analysis using friction model for frictional systems," in *Proc. 2017 IEEE Int. Conf. Mechatron.*, 2017, pp. 37–42.
[29] M. Li, "An integrated model-data-based zero-phase error tracking feedforward control strategy with application to an ultraprecision wafer stage," *IEEE Trans. Ind. Electron.*, vol. 64, no. 5, pp. 4139–4149, 2017.
[30] W. Ohnishi and H. Fujimoto, "Tracking control method for a plant with continuous time unstable zeros: Finite preactuation based on state trajectory regeneration by using redundant order polynomial," in *Proc. 2016 IEEE 55th Conf. Decision Control*, pp. 4015–4020, 2016.
[31] Y. Yazaki, "Reduction of impact force by model prediction and final-state control for a high precision catapult stage," in *Proc. 42nd Annu. Conf. IEEE Ind. Electron. Society*, pp.5101–5106, 2016.
[32] H. Fujimoto and T. Takemura, "High-precision control of ball-screw-driven stage based on repetitive control using n-times learning filter," *IEEE Trans. Ind. Electron.*, vol.61, no.7, pp.3694–3703, 2009.

Yoshihiro Maeda (M'16) received the B.S., M.S., and Dr.Eng. degrees in electrical and computer engineering from Nagoya Institute of Technology (NITech), Japan, in 2004, 2006, and 2011, respectively. From 2008 to 2013, he was a Project Research Associate with Motion System Research Laboratory, NITech. Since 2015, he has been an Associate Professor with the Department of Electrical and Mechanical Engineering, NITech. He was with Denso, Ltd., Japan, from 2006 to 2007 and with Toyota Industries Corporation, Ltd., Japan, from 2013 to 2015, respectively. His research fields are intelligent control design for mechatronic systems, and modeling and compensation for nonlinear friction. Dr. Maeda is a member of the Institute of Electrical Engineers of Japan, the Japan Society for Precision Engineering, and the Society of Instrument and Control Engineers.

Kazuya Harata received the B.S. degree in electric and electrical engineering from Nagoya Institute of Technology (NITech), Japan, in 2018. Currently, he is a Master degree student of the Department of Electrical and Mechanical Engineering, NITech. His current research interests are motion control of frictional servo systems and its related technologies. Mr. Harata is a member of the Institute of Electrical Engineers of Japan.

Makoto Iwasaki (M'92−SM'09−F'15) received the B.S., M.S., and Dr.Eng. degrees in electrical and computer engineering from Nagoya Institute of Technology (NITech), Japan, in 1986, 1988, and 1991, respectively. Since 1991, he has been with the Department of Computer Science and Engineering, NITech. Currently, he is a Professor of the Department of Electrical and Mechanical Engineering. His current research interests are applications of motion control theory and soft computing techniques for motor/motion control. Dr. Iwasaki is a member of the Institute of Electrical Engineers of Japan and the Japan Society for Precision Engineering.